Journal of Theoretical Biology ■ (■■■■) ■■■–■■■

Contents lists available at ScienceDirect

Journal of Theoretical Biology

journal homepage: www.elsevier.com/locate/yjtbi

Slow-wave oscillations in a corticothalamic model of sleep and wake

X. Zhao [a,b,c,d,e,*], J.W. Kim [a,b], P.A. Robinson [a,b,c,d,e]

[a] School of Physics, The University of Sydney, Sydney, New South Wales 2006, Australia
[b] Center of Research Excellence, Neurosleep, 431 Glebe Point Rd, Glebe, New South Wales 2037, Australia
[c] Center for Integrative Brain Function, University of Sydney, New South Wales 2006, Australia
[d] Cooperative Research Center for Alertness, Safety, and Productivity, University of Sydney, New South Wales 2006, Australia
[e] Brain Dynamics Center, Westmead Millennium Institute, University of Sydney Medical School, Westmead, New South Wales 2145, Australia

HIGHLIGHTS

- We model cortical UP/DOWN states using a corticothalamic neural field model.
- We implement bursting dynamics in the reticular nucleus of the corticothalamic model.
- The neural field model is capable of reproducing deep amplitude cortical UP/DOWN oscillations in slow-wave sleep, while also reproducing EEG time series and power spectra characteristic of wake and spindle states.

ARTICLE INFO

Article history:
Received 2 May 2014
Received in revised form
21 January 2015
Accepted 24 January 2015

Keywords:
Slow wave sleep
Neural field theory
Thalamus
Cortex

ABSTRACT

A physiologically-based corticothalamic neural field model is used to study slow wave oscillations including cortical UP and DOWN states in deep sleep by extending it to incorporate bursting dynamics of neurons in the thalamic reticular nucleus. The interplay of local bursting dynamics and network interactions produces the cortical UP and DOWN states of slow wave sleep while preserving previously verified model predictions in the wake state. Results show that EEG spectral features in wake and sleep are reproduced. The bursting is subthreshold but acts to intensify the amplitude of oscillations in slow wave sleep with deep UP/DOWN oscillations on the cortex emerging naturally. Furthermore, there is a continuous cycle between the two regimes, rather than a flip–flop between discrete states.

1. Introduction

Clinically, the most studied range of electroencephalographic (EEG) frequencies is 0.1–100 Hz (Nunez and Srinivasan, 2006). There are numerous characteristic states discernible on the EEG and can allow for the identification of distinct sleep stages, eyes-open and eyes-closed states in wake, depth of anesthesia, seizures, and other neurological disorders. Each state is defined by key rhythms that dominate the EEG. Brain activation is associated with low-amplitude fluctuations at relatively high frequencies in the alpha rhythm which lies between 8 and 13 Hz and is most prominent when subjects are awake with eyes closed. Slow wave sleep (SWS) is dominated by high amplitude, low frequency components. Furthermore, SWS exhibits characteristic UP and DOWN states (≈ 1 Hz) observed in local field measures of the cortex (Sanchez-Vives and McCormick, 2000; Steriade et al., 1993a, 1993b). The UP state involves strong excitation of cortical neurons, whereas cortical neurons are hyperpolarized in the DOWN state. Alternation between cortical UP and DOWN states is observed in local field potential measurements as a slow wave oscillation at ≈ 1 Hz; however, understanding of cortical UP and DOWN states in SWS is still lacking. Numerous competing theories have been proposed that variously involve corticocortical and thalamocortical systems (Andersen and Andersson, 1968; Berger, 1933; Bishop, 1936; Steriade and Deschenes, 1984), but there is no consensus on the exact mechanisms generating the cortical UP and DOWN states.

The major cell populations involved in EEG generation are reticular thalamic neurons, cortical pyramidal cells, interneurons,

* Corresponding author at: School of Physics, The University of Sydney, Sydney, New South Wales 2006, Australia. Tel.: +61 2 9351 5896.
E-mail address: xzha6112@uni.sydney.edu.au (X. Zhao).

http://dx.doi.org/10.1016/j.jtbi.2015.01.028
0022-5193/

and thalamocortical neurons (Steriade et al., 1993a, 1993b; Robinson et al., 1997). Excitation of the reticular thalamic nuclei causes inhibition of the thalamocortical cells in the relay nucleus. This in turn reduces excitation in the cortex, which leads to decreased afferent activity from the cortex back onto the reticular thalamus. This forms a negative feedback loop (Robinson et al., 2002).

Attempts at modeling the cortical UP and DOWN transition in deep sleep have primarily been made using neuronal networks (Bazhenov et al., 2002; Compte et al., 2003; Hill and Tononi, 2005) with most theories focusing on the bursting dynamics of thalamic neurons (Grenier et al., 1998; Steriade and Deschenes, 1984; Steriade et al., 1993a). This emphasizes the "pacemaker" qualities of thalamic neurons (i.e., their ability to fire or burst at a characteristic frequency), and has been extensively modeled in the context of single neurons and small networks (Destexhe et al., 1993, 1994). The approaches have varied from a purely cortical model to thalamocortical interactions. Invariably, the UP and DOWN states are generated from the interaction of single cells in the network, which represent slow wave activity through ion channel and synaptic dynamics. However, these network simulations of UP and DOWN transitions have only simulated on the order of 10^2–10^4 neurons, which is a severe limitation when studying global brain states such as SWS.

An alternative approach is to use neural field theory to average over the microstructure of neuronal connections to yield a neural field model (Deco et al., 2008). Such neural field theories have already accounted for many characteristic states observed on the EEG, such as several stages of sleep, eyes-open, and eyes-closed in wake (Robinson et al., 2004, 2005) plus non-linear dynamics of seizures and other phenomena (Breakspear et al., 2006; Deco et al., 2008; Robinson et al., 2002). Neural field theory based models allow tractable analysis of large-scale brain dynamics. Some efforts at modeling the sleep-wake transition have been previously made using neural field theory (Steyn-Ross et al., 2005). However, the analysis did not extend to the inclusion of bursting dynamics nor corticothalamic feedback. The current work builds upon a neural field model of corticothalamic dynamics (Robinson et al., 2002, 2004) that has previously been successfully used to explore wake and SWS based on physiological parameters (Rowe et al., 2004). These include reproducing characteristic features of the EEG such as alpha and beta spectral peaks and small amplitude, rapid oscillations in the wake state, slow wave oscillations (≈ 1 Hz) and $1/f$ spectrum in the sleep state (Robinson et al., 2002).

Here we extend this neural field theory to explain cortical UP and DOWN transitions in SWS. Our previous work explained some aspects of the SWS oscillation (Robinson et al., 2002), but did not fully generate cortical UP and DOWN states with the prominent depths at low frequencies observed in the current work.

To extend the previously studied neural field model (Robinson et al., 2002, 2004) we incorporate a well-known bursting neuron model (Wilson, 1999a) whose dynamics has previously been expressed in terms of rate-based equations that are compatible with neural field theory (Robinson et al., 2008). We proceed to examine the effects of bursting dynamics in the thalamus on the neural field model and show that our new model is capable of producing cortical UP and DOWN states in SWS while preserving previous results in wake and sleep (Robinson et al., 2002).

This contrasts with previous modeling work that implemented intrinsic rebound bursting in thalamic neurons because we contend that the ≈ 1 Hz oscillation arises from network resonances that couple to the intrinsic bursting dynamics of neurons in the thalamic reticular nucleus, rather than solely arising from the pacemaker properties of rebound bursts. We implement bursting dynamics only in the reticular nucleus because it has been shown to be crucial for the generation of oscillations in the thalamus (Steriade et al., 1985) and is the most parsimonious ansatz. It is possible to add bursting dynamics in other populations such as the thalamic relay nuclei; however, the present work shows that this additional complication is not required to generate cortical UP and DOWN states in SWS. We emphasize that in the current study UP and DOWN states specifically refer to oscillations on the cortex, unless otherwise noted.

Beginning from Section 2 we incorporate bursting dynamics into an existing neural field model. Then we recapitulate the salient features of the neural field model and the parameter states we use for the current work. Following this, in Section 3 we demonstrate the presence of spontaneous UP and DOWN states during SWS dynamics. Subsequently we show the abolition of this behavior as the system shifts to the wake state and reproduces characteristic spectral features of the wake EEG. Thus, in the current work we extend the domain of the neural field model's physiological activity to include UP and DOWN states in SWS while replicating all previous results. We conclude in Section 4 with our main findings and discuss future directions for our neural field model with the incorporation of bursting dynamics.

2. Methods

We begin with a single compartment bursting neuron (Wilson, 1999a) and using previously published results, show how its behavior can be expressed in terms of rate dynamics and incorporated into the reticular thalamus of our neural field model. The bursting dynamics in the reticular thalamus then interacts with the cortex and thalamic relay nucleus through a damped wave equation and dendritic filtering. The current work explores the role of simple bursting dynamics in place of rebound bursting in the reticular nucleus although the difference is not critical in the present context because we only explore parameters that are subthreshold for the bursting dynamics.

2.1. Single neuron model

We briefly introduce the single compartment neuron (Wilson, 1999a), described by

$$C\frac{dV}{dt} = -g(V)(V-V_{Na}) - g_R R(V-V_K) - g_X X(V-V_X) - g_H H(V-V_K) + I_{ext}, \quad (1)$$

where C is membrane capacitance per unit area, V is the membrane potential, and R is a recovery variable. The variables V and R together constitute the fast variables that control the spike shape, while X and H are slow variables, discussed below. Eq. (1) describes changes in the membrane potential V, that arise from interactions of ionic currents, the capacitance C and the externally applied current per unit area I_{ext}. Here, $V_{\rm Na}$ is the Na^+ reversal potential, $V_{\rm K}$ is the K^+ reversal potential, and g_R is the membrane conductance for R, while $g(V)$ represents the Na^+ activation function. The reversal potentials for the slow variables are V_X and V_K, while the conductances for the slow variables are g_X and g_H. The dynamics of the fast variables are described by (1) and

$$\frac{dR}{dt} = -\frac{1}{\tau_R}[R - R_\infty(V)], \quad (2)$$

$$g(V) = \nu_0 + \nu_1 V + \nu_2 V^2, \quad (3)$$

$$R_\infty(V) = 0.79 + r_1 V + r_2 (V - V_3)^2, \quad (4)$$

$$R_\infty(V) = 0.17 + r_2 (V - V_4)^2. \quad (5)$$

Eq. (5) describes activation of K^+ channels, $R_\infty(V)$ is the equilibrium state, and τ_R is the time constant for relaxation of R. The values of the parameters are given in Table 1. Note that we had assigned V_1 and V_2 to $V_{\rm Na}$ and $V_{\rm K}$, respectively, in previous work (Robinson et al., 2008).

Please cite this article as: Zhao, X., et al., Slow-wave oscillations in a corticothalamic model of sleep and wake. J. Theor. Biol. (2015), http://dx.doi.org/10.1016/j.jtbi.2015.01.028

Table 1
Parameters for the four populations: excitatory e, inhibitory i, thalamic relay s, and thalamic reticular r. The parameter values provided in the table are constant across both wake and sleep conditions. Sourced from Robinson et al. (2004).

Quantity	Symbol	Value	Unit
Corticocortical connections e axons			
Range	r_e	86	mm
Axonal velocity	v_e	10	m s^{-1}
Damping rate	$\gamma_e = v_e/r_e$	116	s^{-1}
Corticothalamic loop delay	t_0	85	ms
Population activity e, i, s			
Maximum firing rate	$Q_a^{\max}$	340	s^{-1}
Firing threshold	θ_a	12.92	mV
Threshold spread	σ_a'	3.8	mV
Reticular population activity r			
Critical current density	I_c	0.123	A m^{-2}
Time constant for $\tilde{X}$	$\tau_{\tilde{X}}$	0.15	s
Time constant for $\tilde{H}$	$\tau_{\tilde{H}}$	0.60	s
Normalization constant	a_x	0.003	s
Conductance per unit area	μ	16.0	S m^{-2}
Maximum firing rate	$Q_r^{\max}$	100	s^{-1}
Firing threshold	$\theta_r = I_c/\mu$	7.7	mV
Threshold spread	σ_r'	3.8	mV
Mean external input	$\phi_n(0)$	1.0	s^{-1}
External input noise	$\phi_n(\omega)$	5×10^{-5}	s^{-1}

Eqs. (1)–(5) have been discussed in detail elsewhere (Wilson, 1999a), so we only provide a brief summary here.

As previously discussed (Rinzel, 1985), there are several approximations inherent in (1) and (2). The Na^+ activation instantaneously reaches its equilibrium value $g(V)$, there is no inactivation of the Na^+ channel, and the time constant τ_R is independent of V. Finally, the leakage current has been absorbed into the polynomial representations of $g(V)$ and $R_\infty(V)$. Furthermore, both $g(V)$ and $R_\infty(V)$ are approximated as quadratic functions. These simplifying assumptions are physiologically plausible, as was previously justified in detail (Wilson, 1999b). In the case of $g(V)$ a quadratic function adequately captures the nonlinearity of voltage-dependent Na^+ channel activation. We use the same constants as in Wilson (1999b) which were chosen to provide the best fit of the dV/dt isocline in Rinzel's approximation of the Hodgkin–Huxley equations (Hodgkin and Huxley, 1952). The quadratic form for R_∞ was initially introduced by Hindmarsh and Rose (1984) and was further justified in Rose and Hindmarsh (1989).

The slow variables X and H of the model serve to modulate the bursting behavior by switching the firing on and off, with

$$\frac{dX}{dt} = -\frac{1}{\tau_X}[X - X_\infty(V)], \tag{6}$$

$$X_\infty(V) = x_2(V - V_0)(V - V_W), \tag{7}$$

$$\frac{dH}{dt} = -\frac{1}{\tau_H}(H - 3X); \tag{8}$$

Eqs. (6) and (8) represent approximations to the combined dynamics of slow Ca^{2+} mediated bursting and the slow feedback inhibition respectively (Wilson, 1999b).

2.2. Reduced model

We now seek to reduce the above model to a spike-rate formulation amenable to inclusion with neural field theories. From Robinson et al. (2008) this results in a slowly modulated current I_θ,

$$I_\theta = I_c - 3I_b\tilde{X} + (I_b - I_a)\tilde{H}, \tag{9}$$

$$I_a = I_b - g_H(V_{\text{eff}} - V_K), \tag{10}$$

$$I_b = -g_X(V_{\text{eff}} - V_X)/3, \tag{11}$$

where $\tilde{X}$ and $\tilde{H}$ are variables governed by the differential equations

$$\frac{d\tilde{X}}{dt} = -\frac{1}{\tau_{\tilde{X}}}(\tilde{X} - \tilde{X}_\infty), \tag{12}$$

$$\frac{d\tilde{H}}{dt} = -\frac{1}{\tau_{\tilde{H}}}(\tilde{H} - 3\tilde{X}), \tag{13}$$

$$\tilde{X}_\infty = a_x Q_r. \tag{14}$$

The slow equations (12)–(14) form a closed set for $\tilde{X}$ and $\tilde{H}$. In order to preserve fixed points from previous analysis we choose g_H/g_X such that I_θ given by (9) reduces to I_c at steady states of (12) and (13). When (12) and (13) yield a steady state, $\tilde{H} = 3\tilde{X}$. Substituting this equality into (9) and solving for g_H using (10) and (11) results in

$$\frac{g_H}{g_X} = -\frac{1}{3}\frac{V_{\text{eff}} - V_X}{V_{\text{eff}} - V_K}. \tag{15}$$

This gives $g_H = 2.368 g_X$ for our set of parameters. Using this ratio between g_X and g_H means I_c is not modified at steady states of the $\tilde{X}$–$\tilde{H}$ system. The bursting activity is governed by the time constants $\tau_{\tilde{X}}, \tau_{\tilde{H}}$ and conductances $g_{\tilde{X}}, g_{\tilde{H}}$. The various voltage constants are discussed in Robinson et al. (2008). Values used in the current work are shown in Table 1.

2.3. The neural field model

We now give an overview of the neural field model, which is governed by interactions of four populations: excitatory e, inhibitory i, reticular r, and relay s (Kim and Robinson, 2007; Robinson et al., 2003, 2002). In this model, the firing of cells serves as sources of pulse fields which are treated as the average spike rate in each population. These pulse fields obey damped wave equations as they propagate. In postsynaptic neurons, inputs from the spike rate fields are filtered by dendrites before generating a transmembrane potential at the cell body. In turn, the membrane potential determines the firing rate of the population. The firing rate then propagates to other populations, as summarized in Fig. 1.

2.4. Firing rates

A good approximation for the firing rate produced by the summed voltage at the cell body is Robinson et al. (1997)

$$Q_a = \frac{Q^{\max_a}}{1 + \exp[-(V_a - \theta_a)/\sigma_a']}, \tag{16}$$

where $a = e, i, r$ or s. The maximal firing rate at which the sigmoid firing function saturates is $Q_a^{\max}$, V_a is the average membrane voltage of the population relative to resting, θ_a is the mean neural firing threshold, and $\sigma_a'\pi/\sqrt{3}$ is the standard deviation of this threshold. For the reticular population r we use a sigmoid which saturates at a lower firing rate than the three other populations as this most closely resembles the functional form of the bursting model's firing rate (Robinson et al., 2008), see Table 1.

In the reticular population the current I_θ in (9) is a dynamically changing parameter. It represents an effective firing threshold, but when considering a population of neurons it is smeared out in the form of a sigmoid firing function that determines Q_r, the reticular population's firing rate. We can obtain an equivalent rate-voltage relationship by recalling that the current perturbation I and voltage perturbation ΔV at the soma boundary have the same time course (Koch, 2004), whence $I = \mu V$, where μ is the conductance per unit

Please cite this article as: Zhao, X., et al., Slow-wave oscillations in a corticothalamic model of sleep and wake. J. Theor. Biol. (2015), http://dx.doi.org/10.1016/j.jtbi.2015.01.028

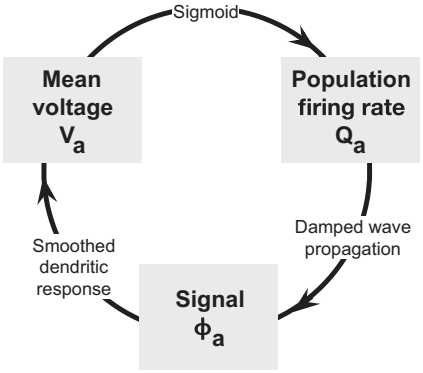

Fig. 1. Summary of the neural field model cycle that determines the interaction of four separate populations. Average cell-body voltage V_a in population a triggers a firing rate Q_a that propagates according to a damped wave equation which gives rise to an afferent signal ϕ_a which is filtered by dendrites to produce a cell-body voltage.

area. Therefore, the threshold voltage θ_r can be obtained from

$$\theta_r = I_\theta/\mu. \tag{17}$$

2.5. Wave propagation

The mean rate of spikes produced by population a is represented by ϕ_a. It is calculated from the firing rate Q_a by the following differential operator:

$$D_a\phi_a = Q_a, \tag{18}$$

which represents the propagation of average firing densities as fields ϕ_a governed by the damped wave equation

$$D_a(\mathbf{r},t) = \frac{1}{\gamma_a^2}\frac{\partial^2}{\partial t^2} + \frac{2}{\gamma_a}\frac{\partial}{\partial t} + 1 - r_a^2\nabla^2. \tag{19}$$

Here, r_a is the mean axonal length for each population a, ν_a is the pulse velocity, and $\gamma_a = \nu_a/r_a$ represents the field damping rate. In the case of ϕ_i, ϕ_r, and ϕ_s, the simplifying assumption $\phi_a = Q_a$ is made because the excitatory cortex is the only population large enough with long distance connections for wave propagation to have a significant effect (Rennie et al., 1999). Hence,

$$\phi_{i,r,s} = Q_{i,r,s}. \tag{20}$$

2.6. Dendritic response

Incoming spikes result in a voltage perturbation at the soma with the form (Koch, 2004; Robinson et al., 1997; Wilson, 1999a):

$$\Delta V(t) = \frac{\alpha\beta}{\beta-\alpha}[\exp(-\alpha t) - \exp(-\beta t)], \tag{21}$$

where (21) has been normalized to unit area and the rate parameters α and β are the decay and rise rate of the soma response, respectively. Standard cable equations imply that the current entering the cell body from the dendritic tree is proportional to minus the spatial derivative of the voltage perturbation at the soma boundary (Koch, 2004). Hence, the form of $I(t)$ induced by a single spike at a synapse has the same form as (21). The total soma voltage perturbation from a train of spikes will be their sum if the effect of the dendritic tree is linear.

The incoming current at the soma is transformed due to the dendritic filtering, with

$$D_{\alpha\beta}V(t) = \phi(t), \tag{22}$$

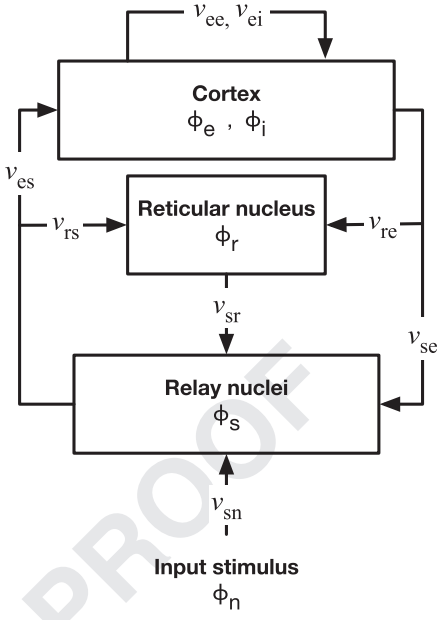

Fig. 2. Schematic of the neural field model with four populations: excitatory e, inhibitory i, thalamic relay s, and reticular thalamus r. From population b the ν_{ab} represent the connection strengths to population a. The population response is ϕ_a, and ϕ_n represents subcortical input, including a noise component.

$$D_{\alpha\beta} = \frac{1}{\alpha\beta}\frac{d^2}{dt^2} + \left(\frac{1}{\alpha}+\frac{1}{\beta}\right)\frac{d}{dt} + 1, \tag{23}$$

where $\phi(t)$ is the time course of the afferent signal and represents the population response. We represent the connectivity strength between two neural populations as $\nu_{ab} = s_{ab}N_{ab}$ where N_{ab} is the mean number of synapses per neuron of population a from neurons of population b, and s_{ab} is the mean strength of synapses. We use the random connectivity hypothesis (Robinson et al., 1998) to exploit symmetries in the connection strengths. Under this hypothesis we assume that the fraction of projections from the source population to each target population is proportional the destination population's size over the total number of neurons projected to. The end result is that $\nu_{ee} = \nu_{ie}$, $\nu_{ei} = \nu_{ii}$ and $\nu_{es} = \nu_{is}$. This implies that $V_i = V_e$ and the inhibitory quantities can be re-expressed in terms of excitatory quantities (i.e., inhibitory effects are not deleted).

A schematic showing the interactions in our neural field model is given in Fig. 2. The thalamic reticular nucleus inhibits relay nuclei. External input stimulus from ϕ_n acts solely on the relay nuclei, which in turn excite both the reticular nuclei and the cortex. Corticothalamic feedback via projections of ϕ_e interacts with the thalamic nuclei. Note that ϕ_n also includes a noise component drawn from a Gaussian distribution. In Table 2 the noise component is expressed in Fourier space, $\phi_n(\omega)$, for $\omega > 0$. The external input stimulus is the zero frequency component $\phi_n(0)$ as shown in Table 1. The pulse rates ϕ_e, ϕ_r, and ϕ_s with their corresponding cell-body potentials then satisfy (Robinson et al., 2003),

$$D_{\alpha\beta}V_e(\mathbf{r},t) = \nu_{ee}\phi_e(\mathbf{r},t) + \nu_{ei}\phi_i(\mathbf{r},t) + \nu_{es}\phi_s(\mathbf{r},t-t_0/2), \tag{24}$$

$$D_{\alpha\beta}V_r(\mathbf{r},t) = \nu_{re}\phi_e(\mathbf{r},t-t_0/2) + \nu_{rs}\phi_s(\mathbf{r},t), \tag{25}$$

$$D_{\alpha\beta}V_s(\mathbf{r},t) = \nu_{se}\phi_e(\mathbf{r},t-t_0/2) + \nu_{sr}\phi_r(\mathbf{r},t) + \nu_{sn}\phi_n(\mathbf{r},t). \tag{26}$$

2.7. Model parameters

The constant parameters of our model are shown in Table 1. These values do not change between different behavioral states such as wake

Please cite this article as: Zhao, X., et al., Slow-wave oscillations in a corticothalamic model of sleep and wake. J. Theor. Biol. (2015), http://dx.doi.org/10.1016/j.jtbi.2015.01.028

Table 2
Dendritic parameters, population connection strengths, and initial values for the $\tilde{X}$–$\tilde{H}$ system in wake and sleep. Sourced from Robinson et al. (2004).

Quantity	Wake	Sleep	Unit
α	83	45	s^{-1}
β	769	185	s^{-1}
ν_{ee}	3.03	4.83	mV s
$-\nu_{ei}$	6.00	4.92	mV s
ν_{es}	2.06	0.78	mV s
ν_{ie}	3.03	4.83	mV s
$-\nu_{ii}$	6.00	4.92	mV s
ν_{is}	2.06	0.78	mV s
ν_{re}	0.33	0.27	mV s
ν_{rs}	0.03	0.02	mV s
ν_{se}	2.18	2.01	mV s
$-\nu_{sr}$	0.83	3.23	mV s
ν_{sn}	0.98	38.30	mV s
g_X	3.0	6.0	A m^{-2}
g_H	7.10	14.2	A m^{-2}
$\tilde{X}_{\text{init}}$	0.0511	0.0642	A m^{-2}
$\tilde{H}_{\text{init}}$	0.1534	0.1925	A m^{-2}

and sleep. Furthermore, they have been chosen to be compatible with known anatomy and physiology (Robinson et al., 2004).

Parameter values in our model have previously been found to be consistent with physiological constraints (Robinson et al., 2002, 2004). However, even within these constraints, only limited classes of behavior are permitted by the form of our equations. Furthermore, the relative effects of population connections change significantly between different arousal states. Thus, each physiological state maps to a well-defined set of ν_{ab} parameters (Robinson et al., 2004). Under these constraints the model unifies many features of EEGs, including spectral peaks in wake and sleep states, evoked response potentials, and seizure dynamics (Rennie et al., 2002; Robinson et al., 2001b, 2002, 2003). We have selected ν_{ab} as tabulated in Table 2. These parameter values have been chosen to be consistent with the ranges found in Robinson et al. (2004).

2.8. Steady states

We are interested in looking for steady states, where the firing rate does not change with respect to time. We can obtain spatially uniform steady states by setting all of the derivatives to zero in (12), (13), (19), and (24)–(26). In (12) and (13) we choose $g_H = 2.368 g_X$ as outlined in Section 2. This reduces (24)–(26) to

$$V_e = \nu_{ee}\phi_e + \nu_{ei}\phi_i + \nu_{es}\phi_s, \tag{27}$$

$$V_r = \nu_{re}\phi_e + \nu_{rs}\phi_{rs}, \tag{28}$$

$$V_s = \nu_{se}\phi_e + \nu_{sr}\phi_r + \nu_{sn}\phi_n. \tag{29}$$

Under the steady state approximation, the firing rate Q_e and ϕ_e are equal because the derivatives have no effect on the damped wave equation. The transcendental equation for steady state firing rates $\phi_e^{(0)}$ is obtained by solving the expressions (27)–(29) to give (Robinson et al., 2004)

$$S^{-1}(\phi_e^{(0)}) - (\nu_{ee}+\nu_{ei})\phi_e^{(0)} = \nu_{es}S\Big\{\nu_{se}\phi_e^{(0)} + \nu_{sr}S\Big[\nu_{re}\phi_e^{(0)} + (\nu_{rs}/\nu_{es})\Big(S^{-1}(\phi_e^{(0)}) - (\nu_{ee}+\nu_{ei})\phi_e^{(0)}\Big)\Big] + \nu_{sn}\phi_n^{(0)}\Big\}, \tag{30}$$

or, equivalently,

$$V_e^{(0)} - (\nu_{ee}+\nu_{ei})S(V_e^{(0)}) = \nu_{es}S\Big\{\nu_{se}S(V_e^{(0)}) + \nu_{sr}S\Big[\nu_{re}S(V_e^{(0)}) + (\nu_{rs}/\nu_{es}) \times \Big(V_e - (\nu_{ee}+\nu_{ei})S(V_e^{(0)})\Big)\Big] + \nu_{sn}\phi_n^{(0)}\Big\}, \tag{31}$$

where the function S^{-1} is the inverse sigmoid defined by

$$S^{-1}(\phi_a) = V_a = \theta - \sigma' \ln\left(\frac{Q_{\max} - \phi_a}{\phi_a}\right). \tag{32}$$

We assume in (30) and (31) that the mean input stimulus $\phi_n^{(0)}$ is constant. Noting that the steady state excitatory potential is $V_e^{(0)} = S^{-1}(\phi_e^{(0)})$, the other steady state firing rates are

$$\phi_r^{(0)} = S\left(\nu_{re}\phi_e^{(0)} + \frac{\nu_{rs}}{\nu_{es}}\Big[V_e - (\nu_{ee}+\nu_{ei})\phi_e^{(0)}\Big]\right), \tag{33}$$

$$\phi_s^{(0)} = S\left(\nu_{se}\phi_e^{(0)} + \nu_{sr}\phi_r^{(0)} + \nu_{sn}\phi_n^{(0)}\right). \tag{34}$$

However, there is now the further complication of $\tilde{X}$ and $\tilde{H}$. If the time derivative for each variable is set to zero then they have no impact on the steady state in (30), because $I_\theta = I_c$ in the steady state for the value $g_H = 2.368 g_X$ used here. This results in $\tilde{X} = \tilde{X}_\infty$ and $\tilde{H} = 3\tilde{X}$. The current paper only studies parameters that are subthreshold for the $\tilde{X}$–$\tilde{H}$ system where this analysis of steady states still applies because the $\tilde{X}$–$\tilde{H}$ system does not alter steady state firing rates. For all simulations in the current paper the neural field model is started at steady state values and the $\tilde{X}$–$\tilde{H}$ system is initialized at $\tilde{X}_{init}$ and $\tilde{H}_{init}$ as shown in Table 2. This is to ensure that the system is within the basin of attraction of the fixed point because the $\tilde{X}$– $\tilde{H}$ system is close to threshold. However, there are parameters for which V_θ traces out a limit cycle when the $\tilde{X}$–$\tilde{H}$ system is supra-threshold, we do not study such cases here except to show an example of the $\tilde{X}$–$\tilde{H}$ alone.

2.9. EEG power spectrum

In our model, the excitatory signal ϕ_e is directly related to the EEG power spectrum because it represents the signal measured at the dendrites after the effects of dendritic filtering represented by (24). This contrasts with V_e, which represents the signal at the *cell-body*. We now show how we obtain time series of local field potentials for each population in our model. In a steady state the system has no temporal variation, so perturbations are required to derive the response. The local field potentials are thus produced by *changes* to ϕ_a. The approach is to perturb the firing rate with noise as given by $\phi_n(\omega)$ for $\omega > 0$.

The power spectrum is given by

$$P(\omega) = \int \frac{d^2\mathbf{k}}{(2\pi)^2} |\phi_e(\mathbf{k},\omega)|^2 F(k), \tag{35}$$

where $F(k)$ is a filter function that accounts for volume conduction through the scalp, skull, and cerebrospinal fluid with Srinivasan et al. (1998)

$$F(k) \approx \exp(-k^2/k_0^2). \tag{36}$$

We have used (35) to calculate the numerical power spectrum from the time series of ϕ_e. In previous work (Robinson et al., 2001a, 2001b; Rowe et al., 2004) we also compared the numerical results with an analytical spectrum. This requires us to consider another 8-dimensional space obtained by multiplying each ν_{ab} by its corresponding ρ_a value to obtain

$$G_{ab} = \rho_a \nu_{ab}, \tag{37}$$

$$G_{ab} = \rho_a s_{ab} N_{ab}, \tag{38}$$

where the gain G_{ab} measures how many additional pulses are generated in population a per input pulse from population b and ρ_a is the sigmoid slope of population a. To find the first order approximation we use a Taylor expansion around the steady state in (31) involving the derivatives of $Q_e = S(V_e)$,

$$Q(\mathbf{r},t) = Q_0 + S'(V_0)[V(\mathbf{r},t) - V_0] + \frac{S''(V_0)}{2!}[V(\mathbf{r},t) - V_0]^2 + \cdots \tag{39}$$

where

$$\phi_a(t) = \phi_a^{(0)} + \rho_a\left(V_a(t) - V_a^{(0)}\right), \tag{40}$$

$$\rho_a = \left.\frac{dS}{dV}\right|_{V_a}, \tag{41}$$

$$\rho_a = \frac{\phi_a}{\sigma'}\left(1 - \frac{\phi_a}{Q_{\max}}\right), \tag{42}$$

where ρ_a is the slope of the sigmoid function evaluated at $V_a^{(0)}$. Applying the perturbation (40) to steady state firing rates causes them to fluctuate versus time. Perturbations result in waves with wave vector $\mathbf{k}$ and angular frequency ω that obey the dispersion relation (Robinson et al., 2001a, 2001b; Rowe et al., 2004)

$$\left(\left[\left(1 - \frac{i\omega}{\gamma_e}\right)^2 + k^2 r_e^2\right](1 - G_{ei}L) - G_{ee}L\right)(1 - G_{srs}L^2) - (G_{ese}L^2 + G_{esre}L^3)e^{i\omega t_0} = 0, \tag{43}$$

where we have

$$q^2 r_e^2 = \left(1 - \frac{i\omega}{\gamma_e}\right)^2 - \frac{1}{1 - G_{ei}L}\left[G_{ee}L + \frac{(G_{ese}L^2 + G_{esre}L^3)e^{i\omega t_0}}{(1 - G_{srs}L^2)}\right], \tag{44}$$

$$L(\omega) = \left(1 - \frac{i\omega}{\alpha}\right)^{-1}\left(1 - \frac{i\omega}{\beta}\right)^{-1}. \tag{45}$$

Here, $G_{ese} = G_{es}G_{se}$, $G_{esre} = G_{es}G_{sr}G_{re}$, and $G_{srs} = G_{sr}G_{rs}$ are the static gains for the relay loop, the reticular and relay loop, and the intrathalamic loop, respectively (Robinson et al., 2002, 2004). We are now able to calculate the analytical spectrum

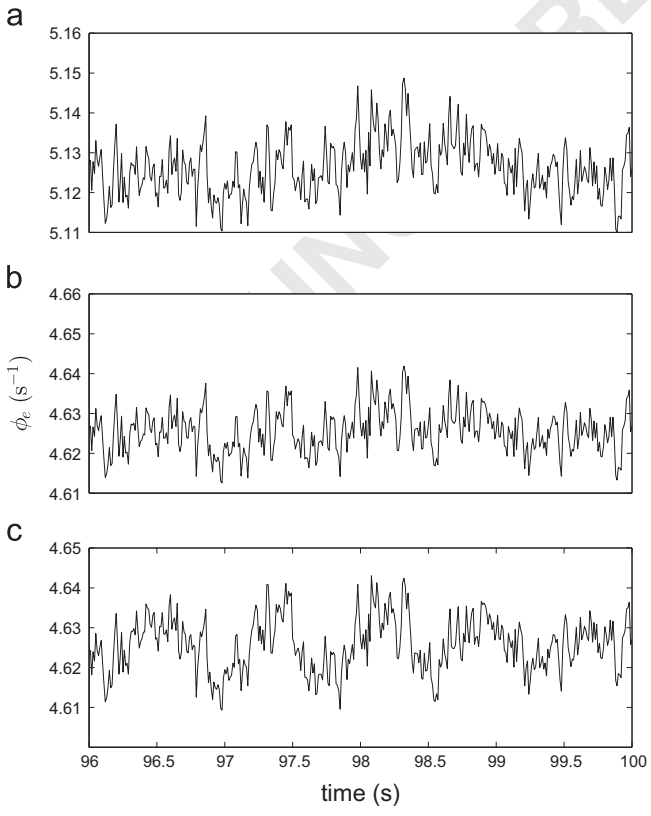

Fig. 3. Fast oscillations seen in cortical ϕ_e in the wake state. A common scale bar shows the amplitude of oscillations. (a) In the original neural field model. (b) For the present model with g_X=3 in the $\tilde{X}$–$\tilde{H}$ system. (c) For the present model with g_X=6 in the $\tilde{X}$–$\tilde{H}$ system.

$$P(\omega) = \left|\frac{G_{esn}L^2}{(1 - G_{srs}L)(1 - G_{ei}L)}\right|^2 \frac{1}{|q^2|^2}. \tag{46}$$

If perturbations to the steady state are small then linear analysis using (37)–(46) is justified and will reproduce the same power spectrum as numerical results (Robinson et al., 2001a, 2001b; Rowe et al., 2004).

3. Results

Connections in our original neural field model were parameterized by the connection strengths ν_{ab} (Robinson et al., 2002, 2004). We have chosen points from this parameter space that produce excellent EEG time series and spectra for wake and sleep. This is then compared with results from our extended neural field model that incorporates bursting dynamics. We emphasize that the ν_{ab} parameters were obtained from the same zones that define specific dynamics such as wake and SWS in the original model (Robinson et al., 2004). We run our simulations close to the steady states for the four populations ($a = e, i, r, s$). The time series are generated from perturbations to the steady state in both the original neural field model and our extended neural field model. We then compare the EEG power spectrum transformed from the local field potential of the cortex. In addition to the power spectrum derived from our time series we also calculate the analytical spectrum. Our results show how our model extends previous findings with the addition of UP/DOWN oscillations in deep sleep while preserving dynamics in other states.

3.1. Time series in wake and sleep

We compare model output with wake time series of corticothalamic model shown in Fig. 3(a). The original neural field model produces features which strongly resemble experimental data with low amplitude, rapid oscillations. When we add bursting dynamics, as shown in Fig. 3(c) and (d), there are minimal changes. This is because the $\tilde{X}$–$\tilde{H}$ system is far from the bursting threshold for wake parameters. The waveform of the time series is very similar, with small changes to the amplitude of the oscillations for both g_X=3 and g_X=6 from interactions with the corticothalamic network. This shows that the general features of the wake time series are preserved at g_X=6.

In Fig. 4 we show the time series in the sleep state for the ν_{ab} in Table 2. Results from our original neural field model are shown in Fig. 4(a). Comparing with those obtained from the extended neural field model in Fig. 4(b) and (c) we immediately observe increased depths of oscillations, most readily seen in Fig. 4(c). This is in contrast with the wake state. In sleep, the corticothalamic network interacts with the bursting dynamics producing slower, high amplitude oscillations. Both are necessary to observe UP and DOWN oscillations, which become more prominent in the sleep parameters up to g_X=6 as shown in Fig. 4(c). We find that g_X=4.5 is an appropriate level to observe UP and DOWN oscillations that correspond well with experimental EEG time series.

The differences in amplitude across Figs. 3 and 4 represent different variations in the mean firing activity of the excitatory cortical population ϕ_e. So, for the wake states shown in Fig. 3 the difference between the maximum firing rate and the minimum firing rate is 0.03 s^{-1} spikes. For the deep sleep states in Fig. 4 the difference between the maximum firing rate and the minimum firing rate for ϕ_e is 0.15–0.4 s^{-1} spikes. This is a reflection of increased amplitude of cortical activity as the arousal state changes through wake, light sleep, and then into deep sleep where cortical UP and DOWN oscillations can be observed.

We provide a close up in Fig. 5 showing the UP and DOWN oscillations for g_X=4.5 along with the parameters governing bursting

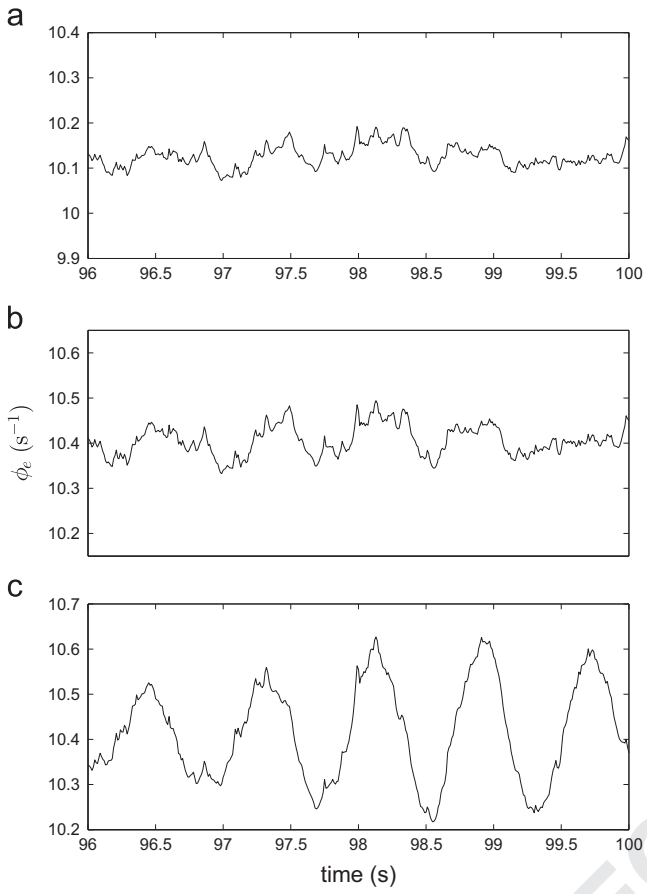

Fig. 4. Slow oscillations seen in cortical ϕ_e in the deep sleep state. A common scale bar shows the amplitude of oscillations. (a) The original neural field model. (b) For the present model with $g_X=3$ in the $\tilde{X}$–$\tilde{H}$ system. (c) For the present model with $g_X=6$ in the $\tilde{X}$–$\tilde{H}$ system.

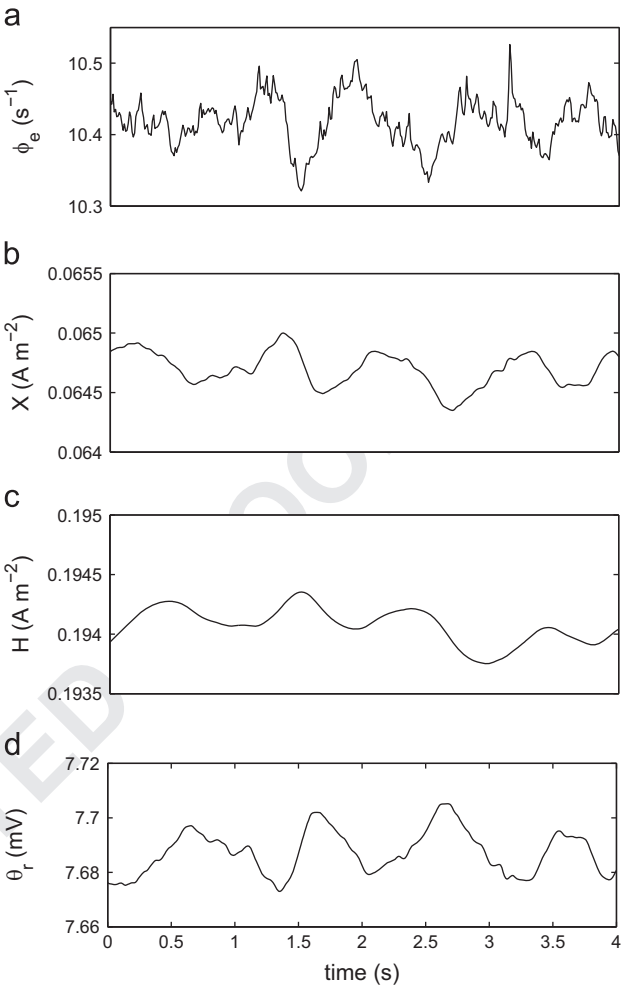

Fig. 5. Slow oscillations observed in neural-field parameters when the reticular nucleus bursting strength is set at the intermediate value $g_X=4.5$. (a) ϕ_e. (b) X. (c) H. (d) θ_r.

in the reticular thalamus. Comparing Figs. 4(a) and 5(a) we observe the same underlying high amplitude, low frequency oscillation of ≈ 1 Hz. However, in the case of Fig. 4(a) the fluctuations around the mean firing rate are smaller in amplitude than Fig. 5(a) and the fluctuations are also less smooth. At $g_X=4.5$ bursting effects cause the oscillations to become more similar to slow wave oscillations. Note that ϕ_e, $\tilde{X}$, $\tilde{H}$, and θ_r are all oscillating with different phases. This is expected as ϕ_e is one of the drivers of the reticular nucleus, $\tilde{X}$ responds to counteract the increase in firing rate of the reticular nucleus, $\tilde{H}$ in turn responds to counteract the increase in $\tilde{X}$ which results in changes seen in θ_r. The changes in θ_r then shift the effective mean firing rate of the reticular population.

Next, we show that the time series produced by our model are comparable to experimental EEG time series. In Fig. 6 EEG time series obtained from healthy controls (D'Rozario et al., 2013) are shown. Comparing Figs. 3(b) and 6(a) reveals the typical low amplitude, fast oscillations observed in the wake state. Furthermore, Figs. 5(a) and 6(b) show the similarities between our model's deep sleep state and that of experimental data where there are high amplitude, low frequency oscillations with smoother time series compared to the wake state. The peak-to-peak amplitudes of the sleep state from our neural-field model, which is measured in terms of population activity (ϕ_e) as shown in Fig. 4 are comparable to the peak-to-peak amplitudes of experimental EEG as can be seen in Fig. 6(b) which is measured in microvolts (μV). Furthermore, low amplitude oscillations observed in the wake state as shown in Fig. 3 are likewise, related to an attenuation of voltage on the experimental EEG as seen in Fig. 6. Hence, there is a high level of concordance of our model's results with experimental data and previous work on our original neural field model (Robinson et al., 2002, 2004).

3.2. Analytical and numerical power spectra

Using parameters in Table 2 we reproduce the alpha and beta peaks typical of a normal wake spectrum in Fig. 7. For comparison we show the linear analytical spectrum in Fig. 7 which was calculated without the $\tilde{X}$–$\tilde{H}$ system. The ν_{ab} used in this example produce a wake spectrum in our original neural field model without bursting dynamics, as shown in Fig. 7(a). Note the close match between the analytical spectrum, calculated without bursting effects, and the numerical spectrum from our original neural field model. This shows that bursting effects are not strong. Furthermore, the spectral peaks are preserved even when bursting is switched on with $g_X=3$ in Fig. 7(a). This is consistent with the similarity of time series shown in Fig. 3(a) and (b).

If we increase the $\tilde{X}$ conductance to $g_X=6$, the power spectrum shows increased power near ≈ 1 Hz, representing an observable difference from the linear analytic spectrum computed without bursting. However, it can be seen that there is very good agreement between the analytical spectrum without bursting and our numerical results for frequency ranges $f \gg 1$ Hz for all g_X studied.

This departure from the linear analytical spectrum without bursting is expected because the $\tilde{X}$–$\tilde{H}$ system accentuates oscillations at ≈ 1 Hz in concert with the network oscillations. This effect

Please cite this article as: Zhao, X., et al., Slow-wave oscillations in a corticothalamic model of sleep and wake. J. Theor. Biol. (2015), http://dx.doi.org/10.1016/j.jtbi.2015.01.028

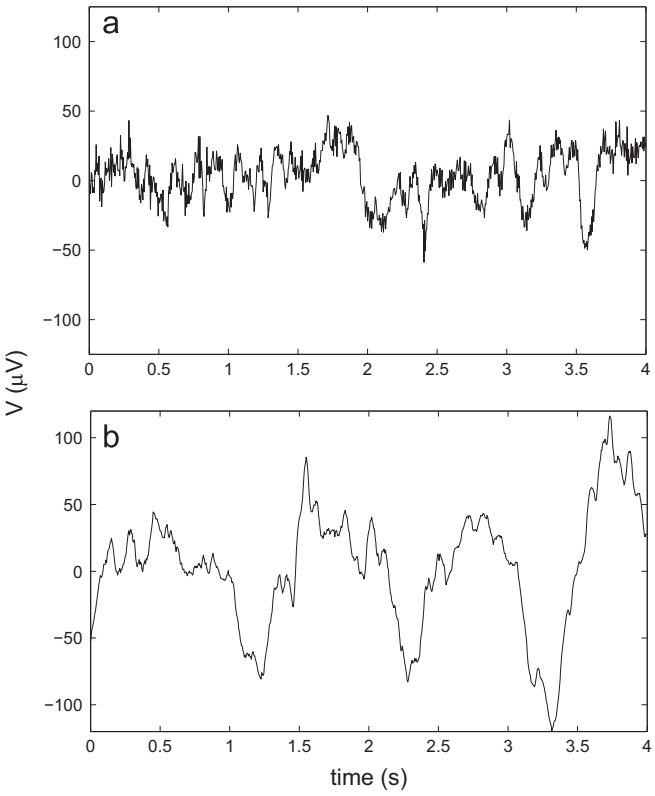

Fig. 6. In vivo recordings of cortical EEG for arousal states. Time series data has been centered on a mean value such that perturbations are relative to 0 μV (a) EEG recording of wake state. (b) EEG recording of sleep state (D'Rozario et al., 2013).

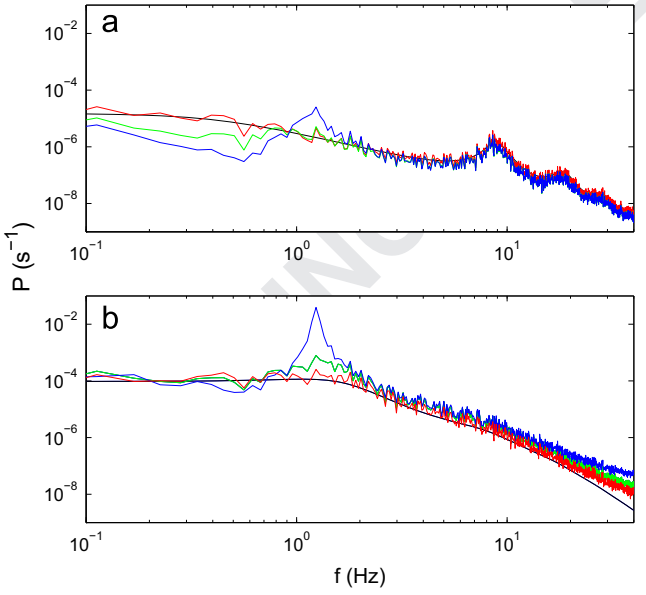

Fig. 7. Power spectra for different parameters. (a) Wake with the analytic spectrum (black), the original neural field model (red), including the $\tilde{X}$–$\tilde{H}$ system with g_X=3 (green), including the $\tilde{X}$–$\tilde{H}$ system with g_X=6 (blue). (b) Sleep with the analytic spectrum (black), the original neural field model (red), including the $\tilde{X}$–$\tilde{H}$ system with g_X=3 (green), including the $\tilde{X}$–$\tilde{H}$ system with g_X=6 (blue). (For interpretation of the references to color in this figure caption, the reader is referred to the web version of this paper.)

is quantified in the next section. More importantly, in the wake state time series in Fig. 3 we do not see any significant deviations from the predictions of the original neural field model in Fig. 3. This is in sharp contrast to the sleep state where UP and DOWN oscillations become more accentuated as g_X increases. This highlights the important role that *both* the bursting dynamics in the reticular population *and* the network oscillations play in shaping UP and DOWN oscillations.

We find that UP and DOWN state transitions arise in the deep sleep state as the strength of $\tilde{X}$ conductance is increased up to g_X=6. We are still able to recover the $1/f$ spectrum in the sleep state at g_X=3. For comparison we show in Fig. 7(b) the analytical spectrum, the numerical power spectrum from the original model, and the numerical power spectrum for g_X=3. For g_X=3, the spectral features closely resemble a $1/f$ power spectrum in the frequency range of 1–6 Hz, while in Fig. 7(b), where g_X=6 the prominence of the 1 Hz oscillation is apparent, with a broad peak at $\approx$1 Hz. This supports the notion that g_X is critically linked to the depth of sleep, and increasing it beyond $g_X \approx 3$ causes UP and DOWN oscillations to emerge. Thus, the extended neural field model captures the states covered by our original model, plus the strong UP/DOWN cycles of SWS.

3.3. *Effects of the $\tilde{X}$–$\tilde{H}$ System*

The effects of the $\tilde{X}$–$\tilde{H}$ system on the neural field model increase with g_X. The dynamics of the $\tilde{X}$–$\tilde{H}$ system show small perturbations away from a steady state, which result in subthreshold oscillations around the fixed point for the arousal states, most obvious in sleep. In wake, the perturbations are extremely small, and the $\tilde{X}$–$\tilde{H}$ system is close to an equilibrium point. However, in sleep the subthreshold perturbations from the fixed point are much larger than in wake, consistent with both our time series and power spectra.

In order to quantify the effects of the $\tilde{X}$–$\tilde{H}$ bursting dynamics on the neural field model we summed the spectral density between 0.5 and 5 Hz for different values of g_X. From the results in Fig. 8 we can quantify the effects if the value for g_X=0 is subtracted from other data points. In agreement with the phase portraits, the bursting dynamics have a much stronger effect in sleep than in wake, as shown in Fig. 8(b) where the power rises significantly more in sleep than in wake for larger values of g_X.

4. Summary and discussion

We have used neural field theory to show that the incorporation of bursting thalamic reticular neurons into a widely tested neural field model is sufficient to generate SWS UP/DOWN oscillations in sleep parameter regions. This work extends the physiological states accounted for by our original neural field model. The main results are

(i) A population averaged bursting-neuron model (Robinson et al., 2008) has been successfully incorporated into our neural field model of corticothalamic dynamics, to represent bursting dynamics in the reticular nucleus of the thalamus.

(ii) The alpha and beta peaks in the wake spectrum and the $1/f$ spectrum characteristic of sleep are preserved in the extended neural field model. For both wake and sleep we use the same connection strengths and parameters as in our previous work for reasons of parsimony and to ensure continuity of the model. The EEG spectra in both wake and sleep are reproduced and accurately represent those seen in experiments. Previous work has already made extensive comparisons between neural field results and experimental data (Robinson et al., 2001b, 2002, 2004; Rowe et al., 2004). Here we have shown that these previous results are retained after the addition of bursting dynamics.

(iii) We have examined the effects of the bursting subsystem and shown that these are stronger in sleep than in wake. These effects relate g_X to the strength of bursting dynamics observed in our extended neural field model. Furthermore, inclusion of the bursting system reproduced accurate wake and deep sleep time series when

Please cite this article as: Zhao, X., et al., Slow-wave oscillations in a corticothalamic model of sleep and wake. J. Theor. Biol. (2015), http://dx.doi.org/10.1016/j.jtbi.2015.01.028

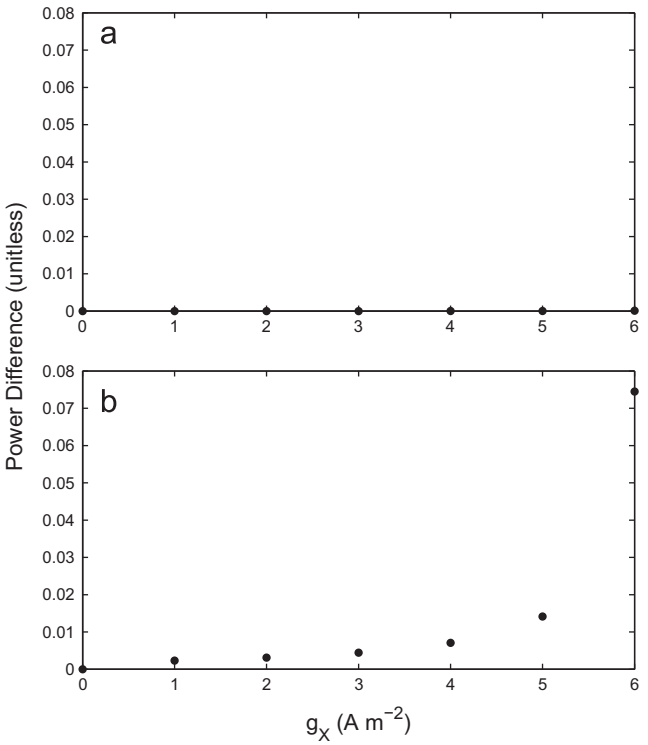

Fig. 8. Spectral power summed over the frequency range 0.5–5 Hz for different values of g_X and then subtracted by the baseline spectral power value given by $g_X=0$, which corresponds to the original neural field model without bursting. Parameters are as in Table 1. (a) Wake state. (b) Sleep state.

compared with experimental EEG recordings. Furthermore, we have shown that bursting dynamics has the most significant effects in deep sleep. The strength of these effects is controlled by the conductance g_X. Increases in g_X cause greater departure from the linear analytical spectrum (calculated without bursting variables $\tilde{X}$ and $\tilde{H}$) as the threshold for self-sustained bursting is approached.

(iv) This study supports the scenario that UP and DOWN oscillations arise from an interplay of network properties and thalamic bursting dynamics because the reticular nucleus is necessary, but not sufficient, to generate the $\approx$1 Hz SWS oscillation. As shown in our results, bursting is only incipient because we do not cross the threshold for the $\tilde{X}$–$\tilde{H}$ system to begin self-sustained bursting. However, the subthreshold perturbations are sufficient to produce UP/DOWN states in an interplay with the corticothalamic network. Thus, we have shown that the dynamics of the bursting variables $\tilde{X}$–$\tilde{H}$ are crucial for the generation of UP and DOWN oscillations.

(v) The existence of UP and DOWN states for deep sleep parameters occurs naturally as g_X is increased. The switching between UP and DOWN states is not separated by discontinuities, rather there are rapid but continuous transitions due to the bursting effects of $\tilde{X}$–$\tilde{H}$. In our original neural field model slow oscillations did exist (Robinson et al., 2005); however, the current work shows the $\tilde{X}$–$\tilde{H}$ bursting system is necessary to intensify the UP/DOWN oscillations to the amplitude seen in experiments.

(vi) Phase portraits further clarify the subthreshold behavior of the $\tilde{X}$–$\tilde{H}$ system and shows why we are able to recover previous results from our original neural field model. In the wake state the $\tilde{X}$–$\tilde{H}$ system is operating very close to a fixed point that does not affect the corticothalamic network. However, due to different corticothalamic network interactions in sleep, the bursting dynamics are stronger, though still subthreshold, which results in UP and DOWN states.

In obtaining the above results we have introduced simple bursting dynamics only in the reticular population because experimental evidence indicates that in vivo the isolated reticular nucleus is capable of generating rhythms in the absence of cortical and thalamic relay input (Steriade et al., 1985), and that corticothalamic oscillations were abolished (Steriade et al., 1987) when the reticular thalamus was lesioned. The most parsimonious model that agrees with these experimental results places the reticular nucleus in a central role for the generation of rhythms in corticothalamic systems, with the cortex–relay–reticular–cortex loop most active in sleep (Robinson et al., 2004) and hence we have focused on bursting dynamics only in the reticular nucleus.

Furthermore, studies have shown that state changes in the brain are accompanied by global release of neurotransmitters that alter connection strengths between different parts of the thalamocortical system (Kandel et al., 2000). These changes also affect the conductances of membrane channels of reticular thalamic neurons, specifically metabotropic glutamate receptors (mGluR), which when activated in association with electrical couplings of neurons in the reticular nucleus led to synchronized rhythms (Long et al., 2004). The mGluR receptors have been implicated in changing low-threshold calcium current, which drives bursting in reticular thalamic neurons (McCormick and Bal, 1997; Turner and Salt, 2003). These effects can be represented by state dependent changes in g_X; hence we have used different values of g_X between wake and deep sleep. Our results indicate that the increase in g_X for the reticular nucleus is tightly linked to global brain state transitions.

In our current model we have included bursting dynamics only in the reticular nucleus. However, thalamic relay neurons are also known to exhibit in vitro bursting behavior; but recent evidence suggests that their behavior is more complex than a simple switching between rapid spiking in wake and low-threshold bursting in sleep (Crunelli et al., 2006). Furthermore, in the current work our main goal was to show that bursting dynamics within the reticular nucleus are sufficient for SWS oscillations to occur for deep sleep parameters. In our model the isolated reticular thalamus does not act as a pacemaker (it is operating at subthreshold levels). Therefore UP/DOWN oscillations arise from thalamocortical network interactions *with* subthreshold bursting dynamics in the thalamus.

Slow EEG oscillations during deep sleep reflect slow membrane potential fluctuations of cortical neurons between UP states and hyperpolarized DOWN states on time scales of 0.5–2 s (Bazhenov et al., 2002). Putative flip–flop transitions have been proposed for numerous stages of sleep (Lu et al., 2006; Saper et al., 2001). Specifically in deep sleep, it has been hypothesized that there is a flip–flop between distinct UP and DOWN states (McCormick, 2005; Mejias et al., 2010). However, in our model UP/DOWN oscillations are not two stable states with a flip–flop transition, rather there is a smooth but rapid transition between the two states. This is a viable picture of UP and DOWN states in deep sleep, as there is scant experimental evidence to support UP/DOWN states as being distinct and stable.

Furthermore, there are several directions to explore using the extended model. Several anesthetic formulations, such as urethane and ketamine–xylazine, can also lead to slow wave oscillations in the EEG, exhibiting UP and DOWN behavior similar to that described for deep sleep (Blethyn et al., 2006), but it is still contentious whether these UP and DOWN states are the same as those observed in deep sleep. By incorporating neuromodulatory effects it would be possible to study the generation of UP and DOWN transitions caused by anesthesia and compare them with the UP and DOWN oscillations observed in the current work. Furthermore, the current neural field model provides noninvasive methods to analyze corticothalamic assemblies by comparing model predictions with clinical observations. This provides a framework to further explore pathologies such as seizures, which may also involve interactions between network oscillations and bursting dynamics.

Please cite this article as: Zhao, X., et al., Slow-wave oscillations in a corticothalamic model of sleep and wake. J. Theor. Biol. (2015), http://dx.doi.org/10.1016/j.jtbi.2015.01.028

Uncited references

Penfield and Erickson (1941), Steriade et al. (2001).

Acknowledgments

We appreciate illuminating discussions with Romesh Abeysuriya. We thank the Woolcock Research Center for permission to use their clinical EEG data. This work was supported by the Australian Research Council, the National Health and Medical Research Council, Westmead Millennium Institute, and Brain Resource.

References

Andersen, P., Andersson, S.A., 1968. Physiological Basis of the Alpha Rhythm. Appleton-Century-Crofts, New York.

Bazhenov, M., Timofeev, I., Steriade, M., Sejnowski, T.J., 2002. Model of thalamocortical slow-wave sleep oscillations and transitions to activated states. J. Neurosci. 22, 8691–8704.

Berger, H., 1933. Über das elektrenkephalogramm des menschen. Eur. Arch. Psych. Clin. Neurosci. 98, 231–254.

Bishop, G., 1936. The interpretation of cortical potentials. In: Cold Spring Harbor Symposia on Quantitative Biology, vol. 4. Cold Spring Harbor Laboratory Press, New York, pp. 305–319.

Blethyn, K.L., Hughes, S.W., Tóth, T.I., Cope, D.W., Crunelli, V., 2006. Neuronal basis of the slow (<1 Hz) oscillation in neurons of the nucleus reticularis thalami in vitro. J. Neurosci. 26, 2474–2486.

Breakspear, M., Roberts, J.A., Terry, J.R., Rodrigues, S., Mahant, N., Robinson, P.A., 2006. A unified explanation of primary generalized seizures through nonlinear brain modeling and bifurcation analysis. Cereb. Cortex 16, 1296–1313.

Compte, A., Sanchez-Vives, M.V., McCormick, D.A., Wang, X.-J., 2003. Cellular and network mechanisms of slow oscillatory activity (<1 Hz) and wave propagations in a cortical network model. J. Neurophysiol. 89, 2707–2725.

Crunelli, V., Cope, D.W., Hughes, S.W., 2006. Thalamic T-type Ca^{2+} channels and NREM sleep. Cell Calcium 40, 175–190.

Deco, G., Jirsa, V.K., Robinson, P.A., Breakspear, M., Friston, K., 2008. The dynamic brain: from spiking neurons to neural masses and cortical fields. PLoS Comput. Biol. 4, e1000092.

Destexhe, A., Babloyantz, A., Sejnowski, T.J., 1993. Ionic mechanisms for intrinsic slow oscillations in thalamic relay neurons. Biophys. J. 65, 1538–1552.

Destexhe, A., Contreras, D., Sejnowski, T.J., Steriade, M., 1994. A model of spindle rhythmicity in the isolated thalamic reticular nucleus. J. Neurophysiol. 72, 803–818.

Grenier, F., Timofeev, I., Steriade, M., 1998. Leading role of thalamic over cortical neurons during postinhibitory rebound excitation. Proc. Natl. Acad. Sci. U. S. A. 95, 13929.

Hill, S., Tononi, G., 2005. Modeling sleep and wakefulness in the thalamocortical system. J. Neurophysiol. 93, 1671–1698.

Hindmarsh, J., Rose, R., 1984. A model of neuronal bursting using three coupled first order differential equations. Proc. R. Soc. Lond. Ser. B: Biol. Sci. 221, 87–102.

Hodgkin, A., Huxley, A., 1952. A quantitative description of membrane current and its application to conduction and excitation in nerve. J. Physiol. 117, 500.

Kandel, E.R., Schwartz, J.H., Jessell, T.M., et al., 2000. Principles of Neural Science, vol. 4. McGraw-Hill, New York.

Kim, J.W., Robinson, P.A., 2007. Compact dynamical model of brain activity. Phys. Rev. E 75, 031907.

Koch, C., 2004. Biophysics of Computation: Information Processing in Single Neurons: Information Processing in Single Neurons. Oxford University Press, New York.

Long, M.A., Landisman, C.E., Connors, B.W., 2004. Small clusters of electrically coupled neurons generate synchronous rhythms in the thalamic reticular nucleus. J. Neurosci. 24, 341–349.

Lu, J., Sherman, D., Devor, M., Saper, C., 2006. A putative flip–flop switch for control of REM sleep. Nature 441, 589–594.

McCormick, D.A., 2005. Neuronal networks: flip–flops in the brain. Curr. Biol. 15, R294–R296.

McCormick, D.A., Bal, T., 1997. Sleep and arousal: thalamocortical mechanisms. Annu. Rev. Neurosci. 20 (1).

Mejias, J.F., Kappen, H.J., Torres, J.J., 2010. Irregular dynamics in up and down cortical states. PLoS One 5, e13651.

Nunez, P.L., Srinivasan, R., 2006. Electric Fields of the Brain: The Neurophysics of EEG. Oxford University Press, USA.

Penfield, W., Erickson, T.C., 1941. Epilepsy and Cerebral Localization. Charles C. Thomas, Baltimore.

Rennie, C., Robinson, P., Wright, J., 1999. Effects of local feedback on dispersion of electrical waves in the cerebral cortex. Phys. Rev. E 59 (3), 3320.

Rennie, C., Robinson, P., Wright, J., 2002. Unified neurophysical model of eeg spectra and evoked potentials. Biol. Cybern. 86, 457–471.

Rinzel, J., 1985. Excitation dynamics: insights from simplified membrane models. FASEB J. 44, 2944–2946.

Robinson, P., Loxley, P., O'Connor, S., Rennie, C., 2001a. Modal analysis of corticothalamic dynamics, electroencephalographic spectra, and evoked potentials. Phys. Rev. E 63, 041909.

Robinson, P., Rennie, C., Rowe, D., O'Connor, S., Gordon, E., 2005. Multiscale brain modelling. Philos. Trans. R. Soc. B 360, 1043–1050.

Robinson, P., Rennie, C., Rowe, D., O'Connor, S., Wright, J., Gordon, E., Whitehouse, R., et al., 2003. Neurophysical modeling of brain dynamics. Neuropsychopharmacology 28, S74.

Robinson, P., Rennie, C., Wright, J., Bahramali, H., Gordon, E., Rowe, D., 2001b. Prediction of electroencephalographic spectra from neurophysiology. Phys. Rev. E 63, 021903.

Robinson, P., Rennie, C., Wright, J., Bourke, P., 1998. Steady states and global dynamics of electrical activity in the cerebral cortex. Phys. Rev. E 58, 3557.

Robinson, P., Wu, H., Kim, J., 2008. Neural rate equations for bursting dynamics derived from conductance-based equations. J. Theor. Biol. 250, 663–672.

Robinson, P.A., Rennie, C.J., Rowe, D.L., 2002. Dynamics of large-scale brain activity in normal arousal states and epileptic seizures. Phys. Rev. E 64, 041924.

Robinson, P.A., Rennie, C.J., Rowe, D.L., O'Connor, S.C., 2004. Estimation of multiscale neurophysiologic parameters by electroencephalographic means. Human Brain Map. 23, 53–72.

Robinson, P.A., Rennie, C.J., Wright, J.J., 1997. Propagation and stability of waves of electrical activity in the cerebral cortex. Phys. Rev. E 56, 826–840.

Rose, R., Hindmarsh, J., 1989. The assembly of ionic currents in a thalamic neuron. I. The three-dimensional model. Proc. R. Soc. Lond. Ser. B: Biol. Sci. 237, 267–288.

Rowe, D.L., Robinson, P.A., Rennie, C., 2004. Estimation of neurophysiological parameters from the waking EEG using a biophysical model of brain dynamics. J. Theor. Biol. 231, 413–433.

D'Rozario, A.L., Kim, J.W., Wong, K.K., Bartlett, D.J., Marshall, N.S., Dijk, D.-J., Robinson, P.A., Grunstein, R.R., 2013. A new EEG biomarker of neurobehavioural impairment and sleepiness in sleep apnea patients and controls during extended wakefulness. Clin. Neurophysiol. 124, 1605–1614.

Sanchez-Vives, M.V., McCormick, D.A., 2000. Cellular and network mechanisms of rhythmic recurrent activity in neocortex. Nat. Neurosci. 3, 1027–1034.

Saper, C.B., Chou, T.C., Scammell, T.E., 2001. The sleep switch: hypothalamic control of sleep and wakefulness. Trends Neurosci. 24, 726–731.

Srinivasan, R., Nunez, P.L., Silberstein, R.B., 1998. Spatial filtering and neocortical dynamics: estimates of eeg coherence. IEEE Trans. Biomed. Eng. 45, 814–826.

Steriade, M., Deschenes, M., 1984. The thalamus as a neuronal oscillator. Brain Res. Rev. 8, 1–63.

Steriade, M., Deschenes, M., Domich, L., Mulle, C., 1985. Abolition of spindle oscillations in thalamic neurons disconnected from nucleus reticularis thalami. J. Neurophysiol. 54, 1473–1497.

Steriade, M., Domich, L., Oakson, G., Deschenes, M., 1987. The deafferented reticular thalamic nucleus generates spindle rhythmicity. J. Neurophysiol. 57, 260–273.

Steriade, M., McCormick, D.A., Sejnowski, T.J., 1993a. Thalamocortical oscillations in the sleeping and aroused brain. Science 262, 679–685.

Steriade, M., Nuñez, A., Amzica, F., 1993b. Intracellular analysis of relations between the slow (<1 Hz) neocortical oscillation and other sleep rhythms of the electroencephalogram. J. Neurosci. 13, 3266–3283.

Steriade, M., Timofeev, I., Grenier, F., 2001. Natural waking and sleeping states: a view from inside neocortical neurons. J. Neurophysiol. 85, 1969–1985.

Steyn-Ross, D.A., Steyn-Ross, M.L., Sleigh, J.W., Wilson, M.T., Gillies, I.-P., Wright, J., 2005. The sleep cycle modelled as a cortical phase transition. J. Biol. Phys. 31, 547–569.

Turner, J., Salt, T., 2003. Group ii and iii metabotropic glutamate receptors and the control of the nucleus reticularis thalami input to rat thalamocortical neurones *in vitro*. J. Neurosci. 122, 459–469.

Wilson, H., 1999a. Simplified dynamics of human and mammalian neocortical neurons. J. Theor. Biol. 200, 375–388.

Wilson, H., 1999b. Spikes, Decisions, and Actions: The Dynamical Foundations of Neuroscience. Oxford University Press, New York.